Journal of Alloys and Compounds 509S (2011) S885–S890

Contents lists available at ScienceDirect

Journal of Alloys and Compounds

journal homepage: www.elsevier.com/locate/jallcom

SIMS study on the surface chemistry of stainless steel AISI 304 cylindrical tensile test samples showing hydrogen embrittlement

C. Izawa[a,*], S. Wagner[a], M. Martin[b], S. Weber[b], A. Bourgeon[c], R. Pargeter[c], T. Michler[d], A. Pundt[a]

[a] Institut für Materialphysik der Universität Göttingen, Friedrich-Hund-Platz 1, 37077 Göttingen, Germany
[b] Gemeinsame Forschergruppe, Helmholtz-Zentrum Berlin/Ruhr-Universität Bochum, Universitätsstr., 150 - IA 2/44, D-44801 Bochum, Germany
[c] TWI Ltd., Granta Park, Great Abington, Cambridge CB21 6AL, United Kingdom
[d] Adam Opel GmbH, 65423 Ruesselsheim, Germany

ARTICLE INFO

Article history:
Received 22 July 2010
Received in revised form
13 December 2010
Accepted 18 December 2010
Available online 28 December 2010

Keywords:
Hydrogen embrittlement
Secondary ion mass spectrometry
Contamination
Oxide layer

ABSTRACT

The local surface chemistry of a low-Ni austenitic stainless steel AISI type 304 used for tensile testing in hydrogen atmosphere is characterized by secondary ion mass spectrometry (SIMS). A chemical map on cylindrical austenitic stainless steel samples can be obtained even after a tensile test. In an effort to obtain the proper chemical element distribution on the samples, the influence of contamination and sample orientation is discussed. An iron oxide on top of a chromium oxide layer is present and Si segregation at grain boundaries is detected. Oxides are judged to reduce the initial hydrogen attack but to be of minor importance for crack propagation during the embrittlement process.

1. Introduction

For the safe use of highly compressed gaseous hydrogen as a fuel, steel fittings, tubes and other components are needed that resist hydrogen embrittlement. Ni-rich austenitic stainless steels show good a resistance to hydrogen embrittlement (HE) but Ni as an alloying element is expensive. For commercial applications, low Ni-content austenitic stainless steels are desired. Results on resistance to HE are unclear for some austenitic stainless steels with concentrations below 10 wt% Ni. For some samples it looks as if there exists a threshold value around 10 wt% Ni [1]. However, tensile tests in hydrogen environment give opposing results, some alloys show HE while other alloys of the same alloy type does not embrittle [2,3]. One possible explanation for this variability is differences in surface layers that may affect hydrogen access to the underlying material. Furthermore, microstructure at the surface is also responsible for HEE. In general, metastable austenitic stainless steels, such as AISI type 301, 304 and 316 transform from austenite to martensite after cold deformation [4,5]. Perng et al. examined hydrogen diffusivity and solubility in annealed and deformed AISI type 301, 304 and 310 [6]. They found that hydrogen diffusivity and permeability in martensite are much higher than in austenite phase. It has been suggested that hydrogen embrittlement of metastable austenitic stainless steels is due to the strain-induced martensite [7–9]. Han investigated the influence of heat treatment on AISI type 304, 316 and 310S austenitic stainless steels [10]. They found precipitation of chromium rich carbides along grain boundaries of the sensitized material, and strain-induced martensite was also observed as a band along grain boundaries. The authors concluded that a zone depleted of chromium and carbon along the grain boundaries reduces the austenite stability during the sensitization. For that reason, we investigated the local chemistry and elemental distribution in solution annealed austenitic stainless steel. In order to investigate the chemical composition of thin surface layers of only several nanometers with the required resolution, surface analysis techniques like X-ray photoelectron spectroscopy (XPS), auger electron spectroscopy (AES) and secondary ion mass spectrometry (SIMS) are useful. In fact, some SIMS studies [11–13] on flat samples have been already carried out. However, detailed studies specifically on as machined and, moreover, tensile-tested specimens of cylindrical shape have not yet been reported.

In this paper we address the local surface chemistry of an austenitic stainless steel with low Ni-concentration by performing SIMS. The samples in this study are as-prepared specimen and solution annealed specimen, respectively. They were subjected to tensile tests in hydrogen gas at 40 MPa and at 20 °C. While the solution annealed sample shows ductile properties in hydrogen atmosphere (Relative Reduction of Area: RRA = 50.1%),

* Corresponding author. Tel.: +49 551 39 5007; fax: +49 551 39 5012.
E-mail addresses: apundt@ump.gwdg.de, chiz1102@googlemail.com (C. Izawa).

0925-8388/$ – see front matter © 2011 Elsevier B.V. All rights reserved.
doi:10.1016/j.jallcom.2010.12.143

Table 1
Chemical composition of the austenitic stainless steel AISI type 304 wt%.

C	Si	Mn	P	S	Cr	Ni	Mo	Cu	V	Co	N
0.016	0.679	1.954	0.030	0.031	17.89	8.63	0.298	0.591	0.092	0.102 0.0713	

the as-prepared sample is more brittle (RRA = 83.9%) [14]. Focus is put on keeping the sample surface in its original condition which means that no further surface polish is allowed. The samples are, therefore, of cylindrical geometry, that possess surface roughness and surface contamination. We will show that even under these conditions reliable SIMS measurements can be performed.

2. Experimental

The commercially available austenitic stainless steel, AISI 304, used in this study was provided by the Deutsche Edelstahlwerke (DEW, Germany) in the form of cylindrical bars with a diameter of 32 mm. The chemical composition is given in Table 1. To ensure the influence of segregation on each specimen to be comparable, only one sample was machined from the centre of the bar parallel to the rolling direction. The bar was machined to a cylindrical sample with a gauge length of 30 mm and a diameter of 5 mm. Due to the machining process, strain induced martensite was obtained on the surface. Thus, the sample was additionally solution annealed in vacuum for 15 min at 1050 °C and quenched with Ar gas at a pressure of 0.2 MPa. The solution annealing process leads to a martensite-free surface. These preparations were carried out in Ruhr-University Bochum, Germany. Tensile tests in 40 MPa hydrogen atmosphere at room temperature have been performed at The Welding Institute (TWI) in Cambridge, England. Afterwards, a typical sample part was cut out in Ruhr-University Bochum and sent to Georg-August-University Göttingen. In Göttingen, the SIMS measurements were performed on the cylindrical surface which was exposed to hydrogen atmosphere.

In SIMS depth profile analysis, surface irregularities cause deterioration in the quality of a depth profile [15]. To examine the influence of the surface roughness on depth profiles, an austenitic stainless steel AISI 304 sample with a diameter of 30 mm was prepared. The sample was solution annealed using the same condition as for the tensile test sample and sliced to semi-cylindrical shape at Ruhr-University. The surface chemistry of the solution annealed samples was addressed to investigate the segregation of elements and the composition of the oxide layer.

A commercial TOF-SIMS IV from ION-TOF GmbH was used equipped with a dual source column (Cs or Ar) as sputtering gun and Ga source as analysis gun. A background pressure of 1×10^{-4} Pa was applied to prevent surface oxidation during the measurement. Details about the SIMS-procedure are as follows.

The tensile tested sample was measured using the surface analysis mode with a Ga^+ primary ion beam at 25 keV which scanned over 500 μm × 500 μm. Afterwards, the surface was sputtered by Ar^+ sputter ion beam scanning over 750 μm × 750 μm at 1 keV to remove the contamination and the oxide layer, respectively. The method enables control of the number of scans at the different depth. This means the distribution of low sensitivity elements can be obtained. The removal process was done by monitoring the signals representing contamination or those representing the oxide layer. The surface analysis was performed, again, on the central region of the sputtered surface.

In order to obtain a depth profile from oxide layer to bulk region, the solution annealed sample was measured by dual beam mode using 25 keV Ga^+ for analysis of 150 μm × 150 μm, and 1 keV Ar^+ or Cs^+ for sample erosion at 300 μm × 300 μm, to get positive or negative secondary ion profiles, respectively. Details about this setup and analysis modes have been published by Iltgen [16].

To obtain a depth length scale, the calibration was carried out by taking following parameters into account. These are (i) a known surface area of sputtering, (ii) the number of ion dose as ion current, (iii) density of iron, (iv) sputtering yield and (v) the time required to remove the oxide layer on an as-machined sample with flat surface. This calibration gives the native oxide layer thickness of about 5 nm, which is in agreement with the previously reported value [17]. The sputter rate and, consequently, the depth scaling for both samples are based on this calibration. Thus, changes in the sputter rate due to different mechanical hardness of the two samples, related to locally different chemical composition and lattice structures, are neglected.

3. Results and discussion

SIMS measurements on tensile tested samples reveal characteristics that need to be regarded with special care. To gain all surface information, measurements were performed without any sample cleaning. Lateral and depth distribution of different elements and possible segregation effects were investigated.

Fig. 1a shows a macroscopic image of the sample after the tensile test in hydrogen atmosphere of 40 MPa. The optical image of the surface is shown in Fig. 1b. The sample surface is still cylindrical and contains many transverse cracks. Fig. 1c is the secondary electron image of the rectangular region highlighted in Fig. 1b. The enlarged secondary electron image verifies a cracked and rough surface with a wavy height modulation. In order to orient the direction of the sample, we defined the transverse direction as the *x*-axis and the longitudinal direction as the *y*-axis. The cracks and the wavy modulation both occur in the *x*-direction.

Secondary ion images of the sample corresponding to the secondary electron image in Fig. 1c are shown in Fig. 2. These images were obtained at different depths eroded by 1 keV Ar^+ bombardment. The uppermost layer of the sample (Fig. 2a) shows high ion intensities for Fe^+, Cr^+ and $Si_2C_5H_{15}O^+$, more or less homogeneously distributed over the sample surface. Crack regions appear dark. The intensity for Ni^+ is low. A high intensity is detected for $C_3F_7{}^+$. Other elements are of minor importance and are not shown here.

After removing the uppermost layer, the intensities of $Si_2C_5H_{15}O^+$ and Fe^+ decrease (Fig. 2b). High intensities are localized in special regions. A correlation between the Fe and the $Si_2C_5H_{15}O^+$ signals can be seen. After removing about 7 nm of surface atoms (Fig. 2c), high intensity regions of Fe^+, Ni^+ and $Si_2C_5H_{15}O^+$ as well as $C_3F_7{}^+$ are detected, whose positions

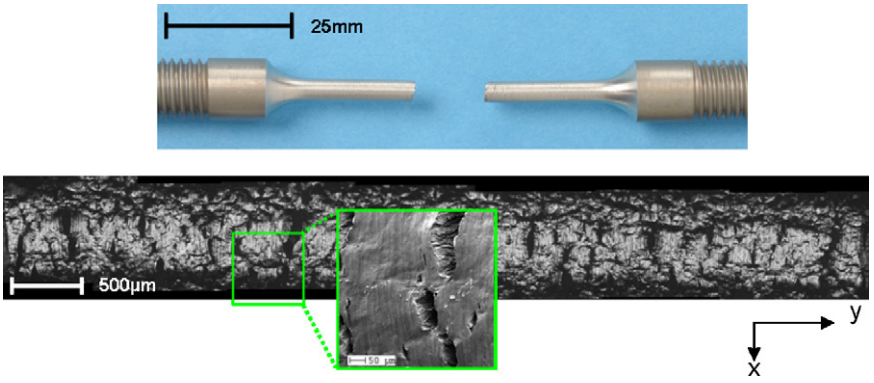

Fig. 1. Austenitic stainless steel sample after tensile test in hydrogen atmosphere of 40 MPa. (a) Macroscopic image, (b) optical image of the surface and (c) secondary electron image of the rectangular region shown in (b). The sample surface is cylindrical and contains many transverse cracks. An enlarged secondary electron image verifies a cracked and rough surface with a wavy height modulation.

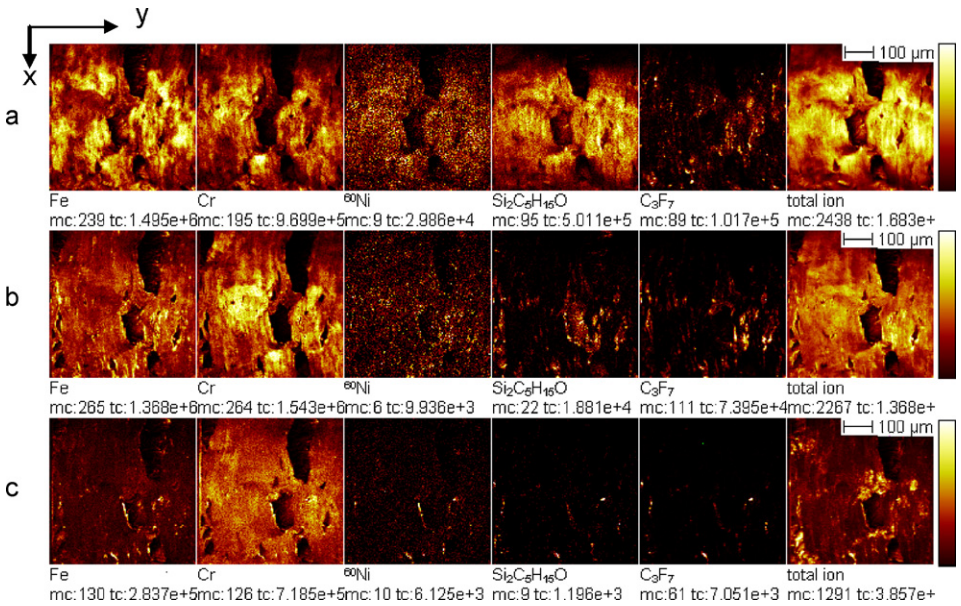

Fig. 2. Secondary ion images of an austenitic stainless steel sample after a tensile test in 40 MPa hydrogen gas. Different sample depth images are shown: (a) uppermost layer, (b) after removing the uppermost layer (at about 0.4 nm), and (c) after removing the oxide layer (at about 7 nm). Color scale is normalized to maximum counts per pixel (mc) for each individual ion. Contamination is visible at all sample depths, especially in crack regions.

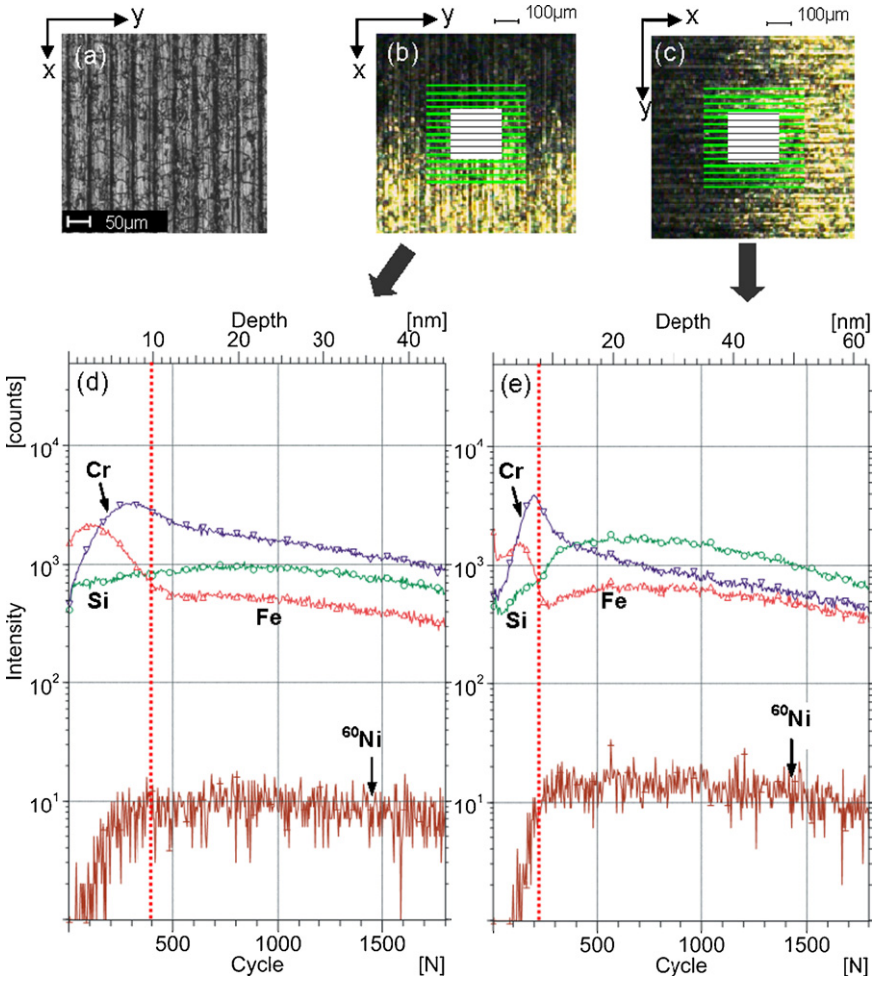

Fig. 3. Depth profiling on the austenitic stainless steel tensile test sample (positive polarity). (a) Macroscopic image and (b and c) CCD camera images. The scanning direction is indicated by green and black lines. The profile depends on the sample orientation, which is (d) perpendicular to surface roughness and (e) parallel to surface roughness. The depth resolution is better for the parallel orientation. (For interpretation of the references to color in this figure legend, the reader is referred to the web version of the article.)

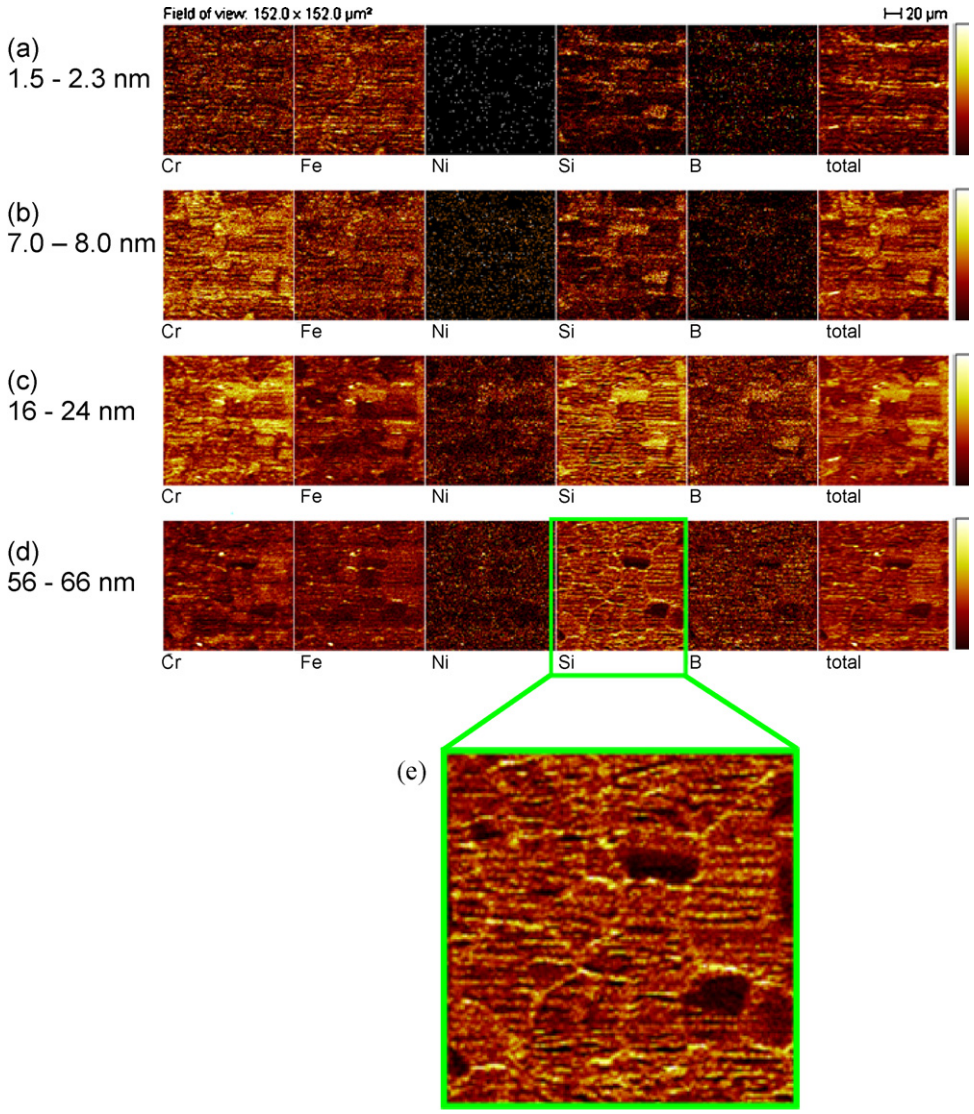

Fig. 4. Secondary ion images of a solution annealed austenitic stainless steel tensile test sample, addressing (a–d) different sample depths regarding Fe^+, Cr^+, Ni^+, Si^+, B^+ and the total element distribution. The measurements are not affected by contamination. (e) Si segregates at grain boundaries.

are highly correlated. $Si_2C_5H_{15}O^+$ and $C_3F_7^+$ are both contamination that hinder a proper determination of the elemental distribution.

A detailed analysis reveals that the $Si_2C_5H_{15}O^+$ signal represents polydimethylsiloxane (PDMS). This originates from the release agent of an adhesive tape that was used to fix the sample for a diameter measurement. Further, PDMS is generally used as a mould-release agent in plastic bags. Plastic bags were used during the sample transfer. The $C_3F_7^+$ signal represents perfluoropolyethers (PFPEs) arising possibly from vacuum oil and machining lubricant. In general, these polymer signals are not critical for depth profiling of a flat sample, because it is possible to remove them by the sputtering process. But here, although the sample was eroded by the Ar^+ beam, contamination is still visible in Fig. 2b and c, especially in crack regions. This results from an uneven sputtering process which is due to the high roughness of the surface. However, the secondary ion formation is strongly influenced by the local chemical state of the surface (matrix effect). Thereby the presence of the contaminations can increase the secondary ion yield, resulting in the high local brightness of the Fe^+, Cr^+ and Ni^+. These images strongly correlate with that of the contamination in Fig. 2c.

In order to obtain proper secondary ion images, the contamination must be removed. For this purpose the commercial austenitic stainless steels (AISI 304 grade) contaminated by PDMS and PFPEs were cleaned in appropriate chemical solutions and were then analyzed by SIMS. It was confirmed that PDMS and PFPEs can be removed by ultrasonic rinsing in hexane and methylene chloride, respectively [18]. By applying this cleaning sequence, reliable elemental distributions can be obtained on as-machined samples.

Furthermore, the tensile test sample contains a wavy height modulation originating from the machining process to achieve the cylindrical shape. This wavy height modulation as well as the cylindrical sample geometry causes a degradation of the depth resolution during depth profiling. Fig. 3a shows an optical image of the sample with a wavy height modulation. The surface roughness is 0.375 µm which is typical for machined samples according to the ASTM standard [19]. To overcome this problem, attention is turned towards the scanning direction of the ion beams. There are two different ion beams used in SIMS: The sputter ion beam and the primary ion beam which are focused at the same position with an incident angle of 45° to the sample surface. Ideal SIMS samples are flat. A curved sample results in a misalignment against both of the sputter and analysis ion beams. In the worst case, the erosion

takes place apart from the analyses. To overcome this problem, the cylindrical sample is oriented with its *y*-direction aligned to both ion beam axes.

The influence of the orientation of these samples on depth profiles is presented in Fig. 3. The sample has large diameter of 30 mm to avoid the discussed sputter gun misalignment due to the cylindrical shape. The wavy surface is maintained. Machining also results in surface contamination that has been removed by sample washing in different chemical solutions prior to the SIMS measurements, as discussed above.

The optical image in Fig. 3a shows that the height modulation has a wavelength of 50 μm. The CCD camera images of the SIMS verify the modulation orientation during the SIMS measurement which is vertical to the scanning direction in Fig. 3b and parallel to the scanning direction in Fig. 3c. Related SIMS depth profiles for Fe^+, Cr, $^+$ Ni^+ and Si^+ are shown in Fig. 3d and e. As can be seen, the broadened depth profiles of Fe^+ and Cr^+ appear for the vertical sample orientation in (d) compared to the parallel sample orientation in Fig. 3e. Vertical dotted lines mark similar features in both figures, visible at 10 nm (Fig. 3d) and at 8 nm (Fig. 3e), respectively. This finding is directly related to the surface roughness. In vertical direction (sample is *y*-oriented), erosion sputtering is pronounced at one side of the modulations, whereas analyze sputtering takes place at the opposite side of the modulation. This effect blurs the depth profile. In the parallel direction (sample is *x*-oriented), erosion and analysis sputtering are possible on the hills and in the valleys of the wavy height modulation. Therefore, the depth profile is sharper and gives the "true" depth profile of the sample surface with higher accuracy. Still, the height modulation widens the depth profile. This effect cannot be prevented when studies on as-machined samples are required. However, surface roughness effects can be minimized by choosing the parallel orientation to the scanning direction.

Fig. 3e shows the best depth profile accessible for solution-annealed samples. It can be seen that Fe^+, Cr^+ and Ni^+ obey a certain layer stacking at the surface. First, a high Fe^+ intensity is detected. Thereafter, at about 3 nm the Cr^+ signal rises. This is followed by the Ni signal at about 8 nm depth. This suggests a stacking sequence of Fe- and Cr-oxides. These will be regarded in more detail by using negative polarity. The Si-intensity is high and reduced in the Fe/Cr-oxide layers.

The lateral elemental distribution of Cr^+, Fe^+, Ni^+, Si^+, B^+ and the sum (total) is shown in Fig. 4, as derived for four different characteristic sample depths (a) 1.5–2.3 nm, (b) 7–8 nm, (c) 16–24 nm and (d) 56–66 nm. Again, the depth scale was obtained by the calibration described in the experimental part. Therefore it is not accurate, especially in the depth of the sample. Grain sizes of about 30 μm are visible in all images. Fe signals are pronounced in (a) while in (b) and (c) the Cr^+ signals dominate. In a depth of 16–24 nm (c) the Ni-signal becomes stronger. Surprisingly, the Si^+ signal also becomes strong, which is even more pronounced in the depth of the sample. As can be seen in the enlarged picture (e) taken from the highlighted Si^+ image in a depth of 56–66 nm (d), Si is located at grain boundaries, cut by coincidence in that image. It is very likely that this is also true for the sample depth shown in (c) where grain boundaries have been crossed in a different way. The interior of some grains in (e) appears dark, confirming the Si segregation at grain boundaries. This Si segregation is suggested to result from the solution annealing, as Si can easily diffuse along grain boundaries.

The ion intensities resulting from the negative polarity are plotted in Fig. 5. Again, the sample is oriented in the optimized *y*-direction. Nitrogen is detected as CNO due to its low sensitivity. The stacking sequence of the FeO^- and CrO^- signal is also visible in the oxide ion image. This confirms the interpretation of a layered stacking of two oxides. Most probably, these oxides are Fe_2O_3 and Cr_2O_3.

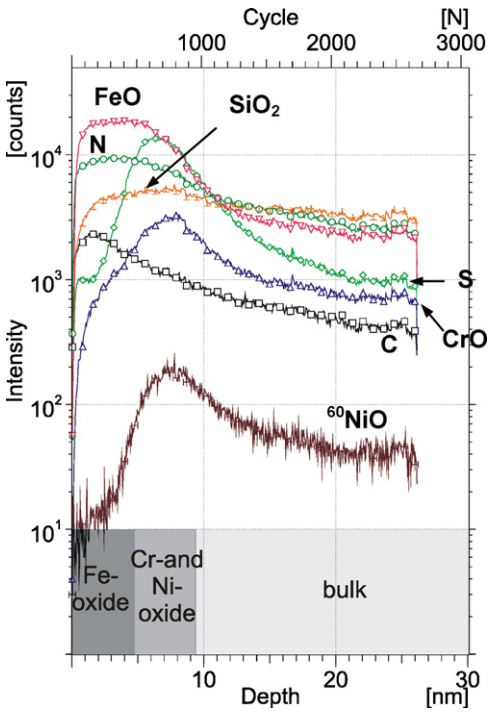

Fig. 5. Depth profiling on an austenitic stainless steel tensile test sample (negative polarity), addressing FeO^-, CrO^-, NiO^-, C^-, N (measured as CNO^-), SiO_2^- and S^-. An oxide stacking is detected at the sample surface.

Furthermore, an increased concentration of nitrogen N^- and Carbon C^- is detected at the sample surface. N content could be related to an impurity in the Ar gas, used for quenching after the solution annealing. However, since the Ar gas contains less than 10 ppm of N, its influence is supposed to be small. The high N concentration most probably arises from the bulk material itself, containing about 0.07 wt%. During solution annealing in high vacuum, N and C could be driven toward the surface and accumulate there. Regarding the high N intensity, there is also the possibility of the SIMS artifact due to the presence of a $^{10}BO_2$ molecular interference at mass 42. Below the Fe-oxide layer a high content of sulfur S is detected, being high at the same depth as the Cr-oxide signal. The SiO_2^- intensity is slightly high in the oxide layer region compared to the bulk region. According to Figs. 4e and 5, a difference in the chemical potential for oxygen directs Si towards the sample surface where oxygen is provided. As a result, Si diffuses from the sample interior to sample surface through grain boundaries during the annealing treatment. Most probably, Si is also oxidized in grain boundaries since the SiO_2^- intensity in Fig. 5 is high even in 26 nm sample depth. On the other hand, the homogeneous distribution of C and N, not shown here, was confirmed in negative ion images. This finding suggested that the diffusion path of C and N differs from that of Si.

This solution annealed sample was found to be rather stable against hydrogen embrittlement [14]. The resistance against embrittlement was interpreted to be due to its surface austenitic phase. Hydrogen diffusion is about three orders of magnitude smaller in the fcc-lattice compared to the bcc-lattice. At 40 MPa, surface oxide layers, additionally, prevent the sample from hydrogen gas exposure. The influence of Si located at grain boundaries on diffusion behavior of hydrogen is not yet clear. However, during the tensile test the surface oxide breaks and brittle crack growth occurs, as it can be seen from Fig. 1. A layered stacking of oxides is found for samples with different surface lattice structure [20]. Therefore, the observed surface oxide and its layer stacking only initially inhibit hydrogen attack. During crack growth it is judged

to be of minor importance for the hydrogen embrittlement process itself.

4. Conclusion

The local surface chemistry of as-machined tensile test samples was analyzed using the SIMS method. This study treated the first characterization of austenitic stainless steel, which is in a cylindrical shape by SIMS. It is possible to study metal and oxide surfaces on cylindrical stainless steel samples even after a tensile test when appropriate conditions are given. These are (a) the surface is solution treated to remove contamination and (b) the sample is oriented to adjust for surface roughness and sample geometry. A layered stacking of Fe- and Cr-oxide with a thickness of 9 nm was found. The solution annealed low-Ni stainless steel is rather resistant against hydrogen embrittlement. This is attributed to the surface phase which is austenitic [14]. Oxides are judged to be of minor importance for the embrittlement process.

Acknowledgment

The authors gratefully acknowledge the financial support of the Bundesministerium für Wirtschaft und Technologie (BMWi) within the project 0327802C.

References

[1] S. Fukuyama, D. Sun, L. Zhang, M. Wen, K. Yokogawa, J. Jpn. Inst. Met. 67 (2003) 56.
[2] A. Barnoush, Doctoral Thesis. Saarbrücken (2007).
[3] A. Pundt, R. Kirchheim, Annu. Rev. Mater. Res. 36 (2006) 555–608.
[4] A.J. McEvily, J.L. Gonzalez Velazquez, Metall. Trans. A 23 (1992) 2211–2221.
[5] A. Miller, Y. Estrin, X.Z. Hu, Scripta Mater. 47 (2002) 441–446.
[6] T.P. Perng, C.J. Altstetter, Acta Metall. 34 (1986) 1771–1781.
[7] G. Schuster, C. Altstetter, Metall. Trans. A 14 (1983) 2077–2084.
[8] T.P. Perng, C.J. Altstetter, Metall. Trans. A 18 (1987) 123–134.
[9] Y. Mine, C. Narazaki, K. Murakami, S. Matsuoka, Y. Murakami, Int. J. Hydrogen Energy 34 (2009) 1097–1107.
[10] G. Han, Acta Mater. 46 (1998) 4559–4570.
[11] P. Williams, C.A. Evans, M.L. Grossbeck, H.K. Birnbaum, Anal. Chem. 48 (1976) 964–968.
[12] M. Grossbeck, H. Birnbaum, Acta Metall. 25 (1977) 135–147.
[13] K. Takai, Y. Chiba, K. Noguchi, A. Nozue, Metall. Mater. Trans. A 33 (2002) 2659–2665.
[14] M. Martin, S. Weber, C. Izawa, S. Wagner, A. Pundt, W. Theisen, Int. J. Hydrogen Energy (submitted for publication).
[15] C.W. Magee, R.E. Honig, Surf. Interf. Anal. 4 (1982) 35–41.
[16] K. Iltgen, J. Vac. Sci. Technol. A: Vac. Surf. Films 15 (1997) 460.
[17] M.G. Ferreira, N.E. Hakikib, G. Goodleta, S. Fatyc, A.M. Simõesa, M.D. Cunha Beloa, Electrochim. Acta 46 (2001) 3767–3776.
[18] J.C. Vickerman, D. Briggs (Eds.), ToF-SIMS: Surface Analysis by Mass Spectrometry, IM Publications LLP, 2001.
[19] H.R. Gray, Hydrogen Embrittlement Testing, ASTM Spec. Technol. Publ., 1974.
[20] J. Langevoort, I. Sutherland, L. Hanekamp, P. Gellings, Appl. Surf. Sci. 28 (1987) 167–179.